In Folio Respiratory Fluxomics Revealed by ^{13}C Isotopic Labeling and H/D Isotope Effects Highlight the Noncyclic Nature of the Tricarboxylic Acid "Cycle" in Illuminated Leaves[1][W]

Guillaume Tcherkez*, Aline Mahé, Paul Gauthier, Caroline Mauve, Elizabeth Gout, Richard Bligny, Gabriel Cornic, and Michael Hodges

Institut de Biotechnologie des Plantes (G.T., A.M., P.G., M.H.), Plateforme Métabolisme-Métabolome IFR87 (G.T., C.M.), and Laboratoire d'Écophysiologie Végétale, Ecologie Systématique Evolution (G.C.), Bâtiment 630, Université Paris-Sud 11, 91405 Orsay cedex, France; and Laboratoire de Physiologie Cellulaire Végétale, Commissariat à l'Energie Atomique-Grenoble, 38054 Grenoble cedex 9, France (E.G., R.B.)

While the possible importance of the tricarboxylic acid (TCA) cycle reactions for leaf photosynthesis operation has been recognized, many uncertainties remain on whether TCA cycle biochemistry is similar in the light compared with the dark. It is widely accepted that leaf day respiration and the metabolic commitment to TCA decarboxylation are down-regulated in illuminated leaves. However, the metabolic basis (i.e. the limiting steps involved in such a down-regulation) is not well known. Here, we investigated the in vivo metabolic fluxes of individual reactions of the TCA cycle by developing two isotopic methods, ^{13}C tracing and fluxomics and the use of H/D isotope effects, with *Xanthium strumarium* leaves. We provide evidence that the TCA "cycle" does not work in the forward direction like a proper cycle but, rather, operates in both the reverse and forward directions to produce fumarate and glutamate, respectively. Such a functional division of the cycle plausibly reflects the compromise between two contrasted forces: (1) the feedback inhibition by NADH and ATP on TCA enzymes in the light, and (2) the need to provide pH-buffering organic acids and carbon skeletons for nitrate absorption and assimilation.

Illuminated leaves simultaneously assimilate (gross photosynthetic assimilation) and produce (photorespiration and day respiration) CO_2. While the general metabolic scheme of the respiratory pathway is known, the regulation of day respiration is one conundrum of plant photosynthetic biology. In fact, day respiration is the cornerstone for nitrogen assimilation by leaves simply because carbon assimilation produces organic materials (carbohydrates) that are in turn converted to nitrogen acceptors by respiration. Unsurprisingly then, intense efforts are currently devoted to elucidate the metabolic basis of the regulation of day respiration, with the optimization of nitrogen assimilation for a better yield of crop plants as an ultimate goal (Lawlor, 2002).

It is well accepted that leaf respiration is often inhibited by light; that is, day respiration is lower than dark respiration (Atkin et al., 2000; Tcherkez et al., 2005, and refs. therein). While there is very little evidence of regulation at the genetic transcription level (Rasmusson and Escobar, 2007), the fundamental reasons invoked to explain such an inhibition by light are enzymatic (posttransductional or biochemical). It has indeed been shown in the unicellular alga *Selenastrum minutum* that pyruvate kinase is inhibited in the light by the high level of cytoplasmic dihydroxyacetone phosphate (Lin et al., 1989). In addition, the mitochondrial pyruvate dehydrogenase complex is partly inactivated by (reversible) phosphorylation in extracts from illuminated leaves (Budde and Randall, 1990; Tovar-Mendez et al., 2003). Photorespiration is probably also involved in the inhibition of pyruvate dehydrogenase, as it has been shown that this enzyme is down-regulated by NH_3, which is a by-product of the photorespiratory Gly decarboxylation (Krömer, 1995). Enzymes of the tricarboxylic acid (TCA) cycle are also assumed to be inhibited in the light because of the high mitochondrial NADH/NAD^+ ratio due to photorespiratory Gly decarboxylation (Gardeström and Wigge, 1988). Additionally, it has been shown that the mitochondrial isocitrate dehydrogenase is inhibited by the high NADPH/$NADP^+$ ratios that may occur in the light (Igamberdiev and Gardeström, 2003; Kasimova et al., 2006). Accordingly, Gly decarboxylase antisense lines of potato (*Solanum tuberosum*) have larger day respiratory decarboxylation rates in the light (as revealed by ^{14}C-labeling experiments), and the ATP/ADP as well as the NADH/NAD^+ ratios are both smaller than in the wild type (Bykova et al., 2005). In addition, the predominance of NADH production by Gly oxidation

[1] This work was supported by the Institut Fédératif de Recherche and the Agence Nationale de la Recherche (Young Researcher Project contract no. JC08–330055 to G.T.).

* Corresponding author; e-mail guillaume.tcherkez@u-psud.fr.

The author responsible for distribution of materials integral to the findings presented in this article in accordance with the policy described in the Instructions for Authors (www.plantphysiol.org) is: Guillaume Tcherkez (guillaume.tcherkez@u-psud.fr).

[W] The online version of this article contains Web-only data.

www.plantphysiol.org/cgi/doi/10.1104/pp.109.142976

over that by the TCA cycle has been shown using isolated mitochondria under ADP-limiting conditions (Day et al., 1985); this might reduce the availability of NAD^+ for the mitochondrial dehydrogenation steps of the TCA cycle. Such a scenario is consistent with the larger in vivo decarboxylation rates of ^{13}C-enriched TCA substrates under very low, nonphysiological oxygen conditions (400 μmol mol^{-1} CO_2, 2% O_2) as compared with high oxygen O_2 conditions (1,000 μmol mol^{-1} CO_2, 21% O_2; Tcherkez et al., 2008).

Physiological experiments have further shown that the inhibition of day respiration in the light is associated with lower TCA cycle activity. When detached illuminated leaves of *Phaseolus vulgaris* were supplied with [^{13}C]1-pyruvate, $^{13}CO_2$ was produced in the light, showing the in vivo activity of pyruvate dehydrogenase; however, when supplied with [^{13}C]3-pyruvate, the ^{13}C labeling in both day-respired CO_2 and citrate was very modest, showing the weak activity of the malic enzyme and enzymes of the TCA cycle (Tcherkez et al., 2005). Oxygen consumption measurements with isolated mitochondria extracted from illuminated spinach (*Spinacia oleracea*) leaves and supplied with exogenous malate, succinate, or citrate showed that citrate gives the lowest respiration rate; in addition, when malate was supplied, it was mainly converted to citrate and pyruvate, with less than 1% isocitrate or fumarate (Hanning and Heldt, 1993). Although the latter results do suggest that TCA cycle reactions were very slow, they also indicate that the phospho*enol*pyruvate carboxylase (PEPC), malic enzyme, citrate synthase, and malate dehydrogenase were still active in the light. It remains plausible that such data obtained in vitro may have been influenced by the experimental extraction-purification of mitochondria as well as the artificial addition of exogenous substrates.

Consequently, then, there is at present no clear picture of day-respiratory fluxomics in illuminated leaves. As an aid to clarifying metabolic fluxes through respiratory reactions and enzymatic regulations in folio, we conducted ^{13}C-labeling experiments in detached leaves of *Xanthium strumarium* (cocklebur) with $^{13}CO_2$, [^{13}C]Glc, or [^{13}C]pyruvate under either D_2O or H_2O conditions. We took advantage of known H/D enzymatic isotope effects to study the metabolic control and the effectiveness of metabolic reactions (Rose, 1961; Rose et al., 1962; Breker et al., 1999; Hochuli et al., 2000). Samples were fixed with the freeze-clamp technique, and the ^{13}C enrichment in metabolites was analyzed with ^{13}C-NMR. Both (1) the effect of D_2O on the ^{13}C distribution and (2) the ^{13}C fluxomic analysis in H_2O indicate that the TCA pathway is not cyclic in the light and is accompanied by rate-limiting steps such as 2-oxoglutarate dehydrogenase and citrate synthase.

RESULTS

Photosynthesis and Transpiration

Figure 1A shows the photosynthetic net CO_2 assimilation value in either H_2O or D_2O, as measured with the open gas-exchange system. Clearly, there was a H_2O/D_2O solvent isotope effect on assimilation of around 2 that corresponds to the H/D isotope effect associated with the carboxylase activity of Rubisco, as already observed by Tcherkez and Farquhar (2008). Both H_2O transpiration measured by the infrared gas analyzer of the gas-exchange system (Fig. 1B) and the estimated $\delta^{18}O$ of water at the evaporative sites (Fig. 1C) demonstrate that leaf water was completely replaced by heavy water in D_2O-fed leaves. (1) In D_2O-fed leaves, transpiration represented less than 10% of that in H_2O-fed leaves; the small value of 0.1 mmol m^{-2} s^{-1} came from the residual infrared absorption of D_2O measured by the infrared analyzer (D_2O absorbance is about 20% of H_2O absorbance at the wavelengths of interest, 2.6–2.8 μm). (2) The estimated oxygen isotope composition of water at the evaporative sites was very close to that of source water (Fig. 1C, dashed lines). As a consequence, all of the recent photosynthetic products formed in the light in D_2O were deuterium labeled. As such, their processing through leaf metabolism was influenced by deuteriation (H/D isotope effects), as will become apparent below.

Leaf CO_2 Evolution

When measured with the method of Laisk (1977; i.e. with CO_2 response curves of net assimilation at different light levels), the CO_2 compensation point in the

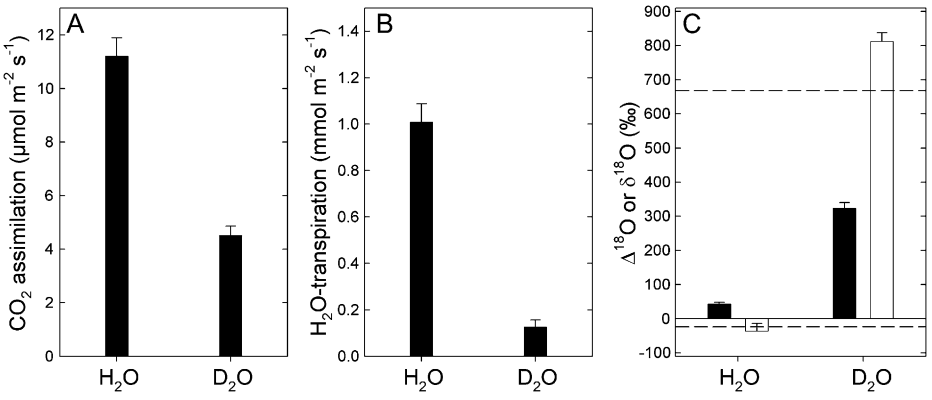

Figure 1. Net photosynthetic assimilation (A), H_2O transpiration (B), photosynthetic $^{18}O/^{16}O$ isotope fractionation (C; $\Delta^{18}O$, black bars), and $^{18}O/^{16}O$ isotope composition of transpired water (C; $\delta^{18}O$, white bars) of detached *X. strumarium* leaves, as photosynthesis operates in H_2O or D_2O under 400 μmol mol^{-1} CO_2, 21% O_2, 400 μmol m^{-2} s^{-1} photosynthetically active radiation, and 21°C. Dashed lines stand for the $\delta^{18}O$ value of source water (H_2O, bottom dashed line; D_2O, top dashed line).

absence of day respiration (Γ*) was similar in natural and heavy water (Fig. 2A). In other words, under a fixed internal CO_2 mole fraction, both H_2O- and D_2O-incubated leaves had the same partitioning factor of Rubisco (v_c/v_o, the carboxylase-to-oxygenase activity ratio); that is, when normalized to CO_2 gross assimilation, photorespiration was similar in both H_2O and D_2O. While there is a small effect of D_2O on the night respiration rate (Fig. 2A), the day respiration rate was reduced by heavy water (Fig. 2B), suggesting that respiratory substrates and/or the metabolic pathway involved in CO_2 evolution (different solvent isotope effects) were not similar in the light and in the dark. In other words, day respiration involved rate-limiting reactions that were isotopically sensitive to deuterium.

Day Decarboxylation of Pyruvate

Detached leaves were fed with ^{13}C-enriched pyruvate in the light under either H_2O or D_2O conditions. The decarboxylation rate of [^{13}C]3-pyruvate and [^{13}C]1-pyruvate via the TCA cycle and the pyruvate dehydrogenase (PDH) was measured using the deviation of the $^{12}C/^{13}C$ on-line photosynthetic isotope fractionation Δ_{obs} due to the production of $^{13}CO_2$ in the light (Fig. 3). In H_2O, the PDH-catalyzed decarboxylation was reduced in the light to a small extent (by nearly 30%) compared with darkness. The decarboxylation associated with the TCA cycle was mostly inhibited (by nearly 75%) by light. In D_2O, both decarboxylations were smaller compared with H_2O either in the dark or in the light.

In the light, there was a solvent isotope effect on decarboxylation rates of about 4 (PDH) or 3 (TCA cycle). The deuterium isotope effect associated with citrate synthase is 3 (Fig. 4; Supplemental Table S1), suggesting that the entry into the TCA cycle was controlled by this very enzyme (similar isotope effect of 3). The deuterium isotope effect of the PDH is smaller (1.7; Fig. 4; Supplemental Table S1) than that observed here (4), so additional deuterium isotope

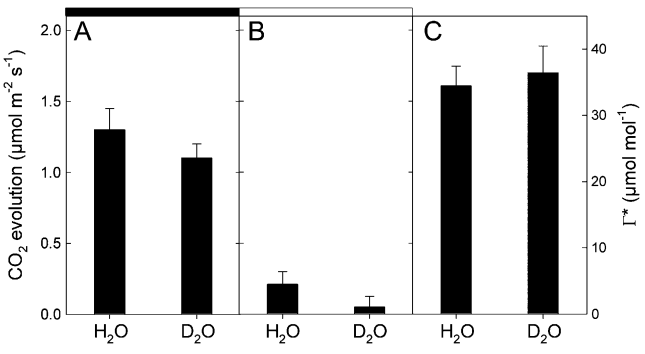

Figure 2. CO_2 evolution of detached *X. strumarium* leaves in either H_2O or D_2O in the dark (A) or in the light (B) at 21°C and 21% O_2. The CO_2 compensation point in the absence of day respiration (c_i-based Γ*) is shown in C. The rate of day respiration (CO_2 evolution in the light) and Γ* were measured with the Laisk method (Laisk, 1977).

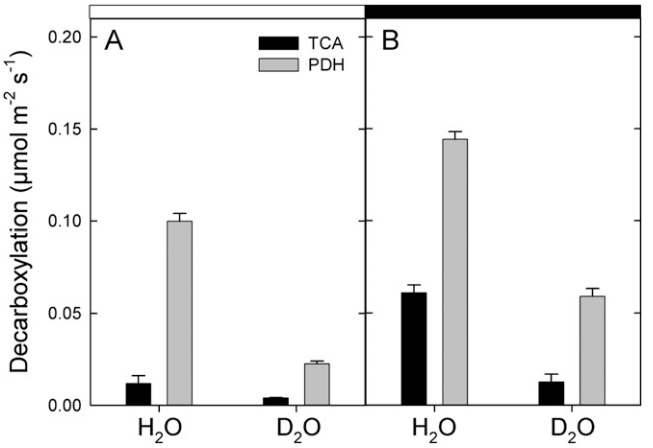

Figure 3. Rate of decarboxylation of ^{13}C-enriched pyruvate by the TCA cycle (black bars) or pyruvate dehydrogenase (gray bars) of detached *X. strumarium* leaves either in the light (A) under 400 μmol mol^{-1} CO_2, 21% O_2, 400 μmol m^{-2} s^{-1} photosynthetically active radiation, and 21°C or in the subsequent dark period (B). The experiments were done in either H_2O or D_2O. The decarboxylation rates were measured using the [^{13}C]pyruvate enrichment technique and subsequent ^{13}C analysis of evolved CO_2 (for details, see "Materials and Methods").

effects occurred, thereby decreasing the $^{13}CO_2$ production from [^{13}C]1-pyruvate. The latter effect may have come from the refixation of $^{13}CO_2$ by the PEPC that impeded the apparent CO_2 evolution by the PDH (see below).

In darkness, the PDH-catalyzed decarboxylation was significantly less affected by D_2O than in the light, with a solvent isotope effect of around 2, which is close to the in vitro deuterium isotope effect (1.7). The TCA cycle is associated with a large isotope effect (nearly 4) in the dark. This value is larger than that of citrate synthase (3), indicating that other effects occurred in D_2O, such as the concatenation of H/D isotope effects along the TCA cycle (i.e., there were cumulative H/D isotope effects on citrate synthase, succinate dehydrogenase, etc.). Therefore, at this stage, the results suggest that under D_2O conditions, the TCA cycle was mainly restricted by citrate production in the light and by several steps in the dark.

Day Respiratory Fluxome

In order to get insight into actual metabolic fluxes associated with day respiration, leaves were labeled with $^{13}CO_2$ in the light and sampling was done with the freeze-clamp technique. The ^{13}C distribution in metabolites was analyzed by NMR. The probability coefficients were back-calculated from the ^{13}C distribution after $^{13}CO_2$ photosynthetic labeling in H_2O. They are shown in Figure 4 (in red). Such calculations included a citrate store at natural abundance (1.1% ^{13}C). Without such a pool, the sum of squares could not be minimized satisfactorily ($S > 0.01$; see "Materials and Methods"). Under the citrate-store assumption, the probability that such a citrate reserve was used to

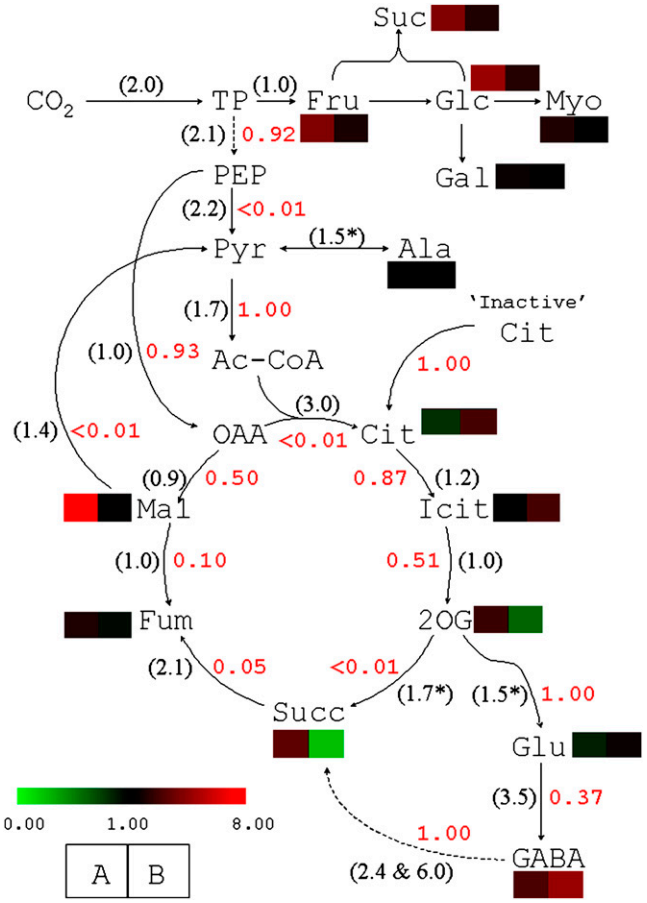

Figure 4. Respiratory fluxome analysis after $^{13}CO_2$ labeling and measurement of ^{13}C enrichments in C-atom positions in metabolites with ^{13}C-NMR on detached *X. strumarium* leaves. CO_2 labeling was done under 400 μmol mol^{-1} CO_2, 21% O_2, 400 μmol m^{-2} s^{-1} photosynthetically active radiation, and 21°C. Transmission coefficients of metabolic reactions (F_j values) are indicated in red. The in vitro H/D isotope effects associated with the enzymes of interest are indicated in parentheses. Colored cells indicate the observed H_2O/D_2O effect on the average molecular ^{13}C enrichment (cell A) and the metabolite concentration measured with gas chromatography coupled to time-of-flight mass spectrometry (cell B). Asterisks indicate that the isotope effect has not been measured, so assumed values obtained with comparable enzymes are shown. Corresponding references for H/D isotope effects are given in Supplemental Table S1.

feed the TCA cycle was 1 and the sum of squares was less than 10^{-4}.

Clearly, two rate-limiting reactions appeared within the glycolytic/respiratory pathway, namely, pyruvate kinase and citrate synthase; their probability coefficient was lower than 0.01 (Fig. 4). In other words, the very modest ^{13}C labeling in citrate and metabolites downstream (e.g. succinate) was such that the calculated probability coefficient of citrate synthase was very small. Both phospho*enol*pyruvate and 2-oxoglutarate were associated with two competitive reactions, for which the PEPC-catalyzed carboxylation and the GOGAT-catalyzed Glu production were much more likely (probability coefficient of 0.93 and 1.00, respectively) than pyruvate kinase and 2-oxoglutarate decarboxylation (probability coefficient < 0.01), respectively. Unsurprisingly, then, the ^{13}C-labeling pattern observed in succinate was consistent with the involvement of the γ-aminobutyrate (GABA) shunt; that is, we found probability coefficients of 1 for 2-oxoglutarate amination and GABA conversion to succinate and of 0.37 for Glu decarboxylase. Noteworthy, oxaloacetate molecules were not fully committed to the citrate synthase reaction but, rather, to malate production (probability coefficient of 0.5) through the reverse operation of the malate dehydrogenase, which was further followed by the fumarase (probability coefficient of 0.1). This result was further confirmed by the use of two transfer coefficients (forward and backward) for both the fumarase and the malate dehydrogenase. Under the assumption that reversibility occurred, the forward transfer coefficients obtained were zero for both reactions with no change of backward values, thereby pointing out that these reactions did operate in a reverse manner (toward fumarate and malate, respectively). As both malate and succinate gave fumarate, fumarate tended to accumulate, as already observed in this species (Tcherkez et al., 2008).

Such a pattern was consistent with the effect of D_2O on the distribution of the ^{13}C label and on metabolite concentrations (Fig. 4, colored cells). First, the most visible effects of D_2O were on sugars and malate. In the latter metabolite, this was due to the lower ^{13}C enrichment in phospho*enol*pyruvate (PEPC substrate) because of the deuterium isotope effect on photosynthetic CO_2 assimilation. Citrate appeared slightly more ^{13}C enriched though slightly less abundant in D_2O. This suggests the involvement of the malic enzyme, which produced ^{13}C-enriched pyruvate from PEPC-derived malate, while the deuterium isotope effect of citrate synthase restricted even more the citrate production rate, thereby reducing its content. Succinate tended to accumulate (larger content; Fig. 4, green color) simply because of the deuterium isotope effect on succinate dehydrogenase. The effect of D_2O on fumarate was very slight but similar to that in malate (slightly less ^{13}C enriched; Fig. 4).

^{13}C Distribution after Pyruvate or Glc Labeling

The ^{13}C percentage in C-atom positions detected with NMR after [^{13}C]pyruvate or [^{13}C]Glc labeling in either H_2O or D_2O is shown in Figure 5, in which values are represented with colors in an isotopomic array. As expected, hexoses, Suc, raffinose, and myo-inositol were labeled after [^{13}C]Glc labeling in H_2O. After [^{13}C]1-pyruvate labeling in H_2O, several atom positions were labeled, including sugars, indicating the refixation of $^{13}CO_2$ evolved from [^{13}C]1-pyruvate. Fumarate was ^{13}C labeled after [^{13}C]Glc feeding in H_2O and not in D_2O. Such labeling may have originated from either the photosynthetic input through the PEPC activity or the TCA cycle, as CO_2 assimilation, glycolysis, and the citrate synthase are affected by a

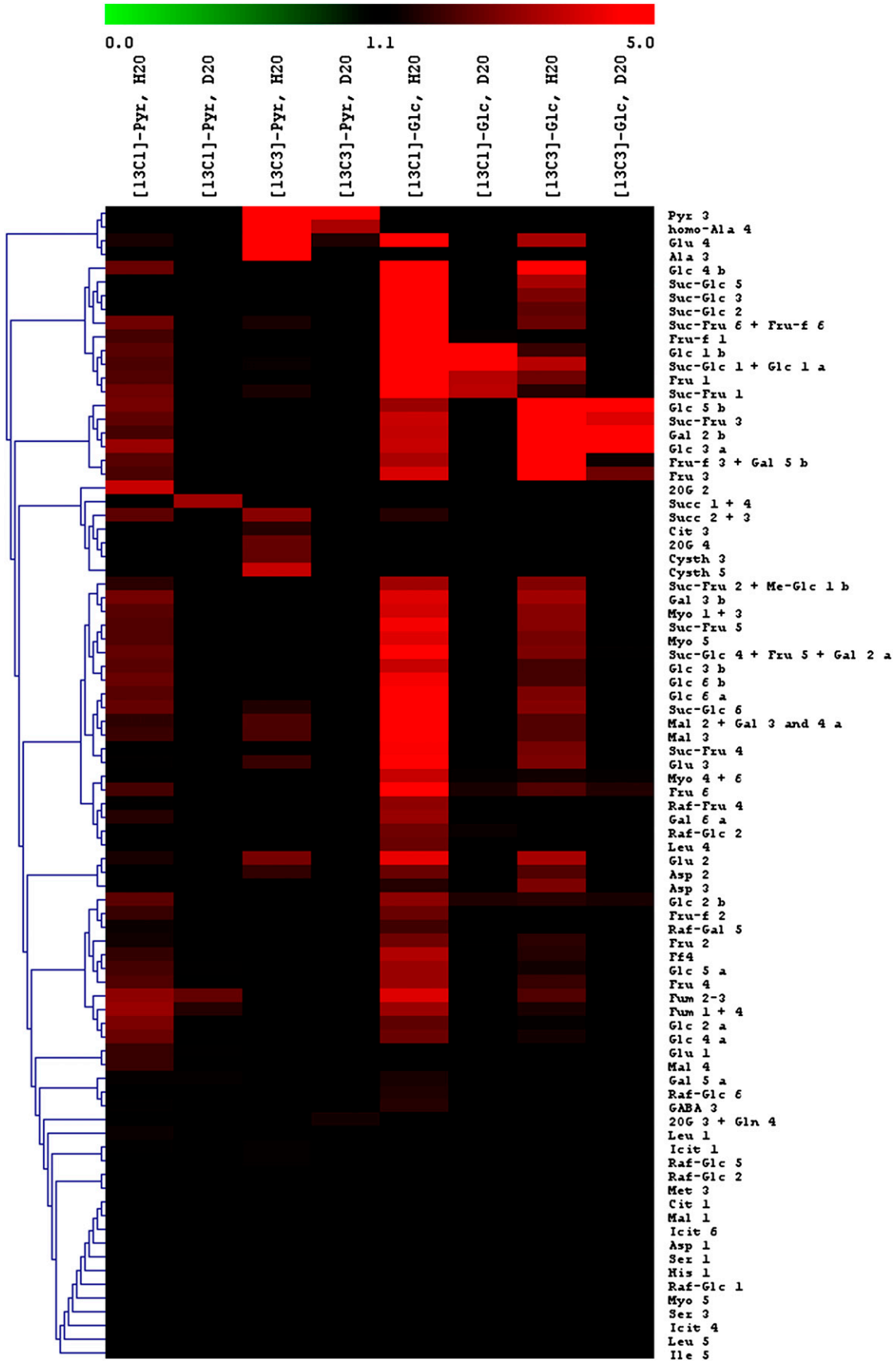

Figure 5. (*Legend appears on following page.*)

deuterium isotope effect. Nevertheless, with [^{13}C]1-pyruvate in H_2O, fumarate was labeled through refixation, while this was not the case with [^{13}C]3-pyruvate, demonstrating that the TCA cycle activity was very small and that the PEPC activity was responsible for fumarate production. Consistently, fumarate was labeled by [^{13}C]1-pyruvate in D_2O, and this was most likely due to the PEPC (re)fixation, which was not affected by deuterium (no H/D isotope effect; Fig. 4), in clear contrast with the TCA cycle. In D_2O, the ^{13}C enrichment in malate showed a quite similar pattern, with (1) labeling in the C-2 and C-3 atom positions by [^{13}C]Glc (through the PEPC activity) and, accordingly, (2) labeling in the C-4 atom position via the refixation of $^{13}CO_2$ evolved from [^{13}C]1-pyruvate.

By contrast, succinate was not labeled with [^{13}C]3-Glc, whereas it appeared labeled by either [^{13}C]1-pyruvate (PEPC refixation) or [^{13}C]3-pyruvate (TCA cycle activity). Citrate showed the same pattern, as did 2-oxoglutarate and Glu. The C-2 and C-3 atom positions of Glu appeared in the same cluster as the C-2 and C-3 atom positions in malate and many C atom positions in carbohydrates, while the C-1 atom of Glu was very close the C-4 atom position in malate. This indicated the important PEPC anapleurotic contribution to providing carbon atoms for Glu synthesis. On the other hand, the labeling of the C-4 atom position in Glu, mainly by [^{13}C]3-pyruvate, was inherited from the labeling in 2-oxoglutarate formed by the TCA cycle. In addition, the C-4 atom position in Glu formed a cluster with Ala and homo-Ala, which are immediate sink metabolites after [^{13}C]pyruvate feeding. In other words, Glu was one major carbon sink to which organic acids (citrate, isocitrate, 2-oxoglutarate) of the TCA cycle were channeled.

The ^{13}C Relationship between Succinate and Fumarate

As an aid in clarifying the metabolic relationship between TCA metabolites, a graph showing the ^{13}C enrichment in fumarate versus that in succinate (data redrawn from Fig. 5) is shown in Figure 6. These two metabolites were chosen here because fumarate follows succinate within the TCA cycle, while they may have different C-atom origins: the PEPC activity and the backward catalysis by fumarase, or the forward operation of the TCA cycle. It is clear that fumarate and succinate did not have a similar ^{13}C enrichment pattern, some data being far from the 1:1 relationship. Rather, two different cases were observed: (1) a weak labeling in succinate combined with an increasing labeling in fumarate (Fig. 6, bottom group), and (2) a nearly constant ^{13}C labeling in succinate combined with a similar or lower labeling in fumarate (Fig. 6, top group). Such groups matched two different labeling conditions: [^{13}C]3-pyruvate (top group) and [^{13}C]Glc or [^{13}C]1-pyruvate (bottom group). This coincidence indicates that the ^{13}C label in products of CO_2 (re)fixation and carbohydrates could reach fumarate molecules but not succinate. By contrast, the production of excess [^{13}C]acetyl-CoA after [^{13}C]3-pyruvate labeling fed TCA intermediates downstream, such as succinate. In other words, there was a disequilibrium of the ^{13}C label distribution between the PEPC-derived fumarate and the forward steps of the TCA cycle that produce succinate. After [^{13}C]3-pyruvate labeling in D_2O, the ^{13}C labeling in succinate virtually disappeared (Fig. 6, white circles), likely because of the citrate synthase restriction (H/D isotope effect). This is not the case for fumarate for one datum (approximately 2.5% ^{13}C), indicating again that the ^{13}C enrichment in fumarate was weakly citrate synthase dependent.

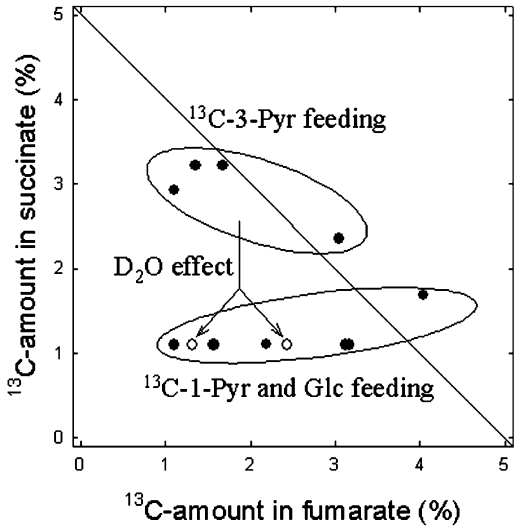

Figure 6. Relationship between the ^{13}C enrichment (percentage) in C-atom positions in fumarate and the symmetrical C-atom positions in succinate (i.e. C-2 + C-3 and C-1 + C-4). Only data in which one of these two metabolites was labeled ($^{13}C > 1.1\%$) are shown. Black circles, H_2O conditions; white circles, D_2O conditions. Pyr, Pyruvate.

DISCUSSION

Although it has become widely accepted that leaf day respiration is inhibited in the light, the importance of respiratory TCA cycle reactions for leaf photosyn-

Figure 5. Isotopomic array representation of ^{13}C enrichment in C-atom positions detected with ^{13}C-NMR after [^{13}C]Glc or [^{13}C]pyruvate labeling of *X. strumarium* leaves in either H_2O or D_2O in the light under 400 μmol mol^{-1} CO_2, 21% O_2, 400 μmol m^{-2} s^{-1} photosynthetically active radiation, and 21°C. Cit, Citrate; Cysth, cystathionine; Fum, fumarate; Icit, isocitrate; Mal, malate; Me-Glc, *O*-methyl-Glc; Myo, myoinositol; Pyr, pyruvate; Raf, raffinose; Succ, succinate; 2OG, 2-oxoglutarate. Fru is designated as Fru (pyranic form) or Fru-f (furanic form). Carbon atom positions are indicated with numbers. Suc-Glc indicates the Glc moiety of Suc, Raf-Glc indicates the Glc moiety of raffinose, and so on. Lowercase a and b indicate α- and β-configurations of hexoses, respectively.

thesis has been recognized (Nunes-Nesi et al., 2007); furthermore, there are many uncertainties on whether the TCA cycle biochemistry is similar in the light compared with the dark. Here, we investigated the metabolic fluxes of individual reactions of the TCA cycle in intact detached leaves of *X. strumarium* with two isotopic methods (^{13}C fluxomics and H/D isotope effects).

The TCA Cycle Comprises Rate-Limiting Steps

The respiratory fluxome was calculated from the ^{13}C enrichment in metabolites after $^{13}CO_2$ feeding. While we recognize that such ^{13}C enrichment values are associated with whole-cell metabolite pools and not specific mitochondrial, chloroplastic, or cytoplasmic pools, several limiting steps clearly accompanied CO_2 evolution in the light at the leaf level: pyruvate kinase, citrate synthase, and 2-oxoglutarate dehydrogenase (probability coefficient < 0.01; Fig. 4). Accordingly, phospho*enol*pyruvate was consumed by the PEPC, 2-oxoglutarate was consumed by the GOGAT to produce Glu, and the citrate pool was supplemented by the remobilization of stored citrate (Fig. 4). Similar conclusions were reached with the use of heavy water. First, day respiration was strongly affected by D_2O, indicating that rate-limiting respiratory reactions are sensitive to deuterium (H/D isotope effect; Fig. 2). Second, [^{13}C]pyruvate decarboxylation by the TCA cycle ($^{13}CO_2$ production from [^{13}C]3-pyruvate) was associated with a H_2O/D_2O isotope effect of nearly 3 in the light, a value similar to that of citrate synthase (Fig. 3). Third, [^{13}C]pyruvate decarboxylation by the PDH ($^{13}CO_2$ production from [^{13}C]1-pyruvate) was associated with a H_2O/D_2O isotope effect of nearly 4 in the light, much larger than that of the PDH alone (1.7). This indicates that in D_2O, $^{13}CO_2$ evolved from [^{13}C]1-pyruvate was either consumed by PEPC-catalyzed refixation or diluted by $^{12}CO_2$ evolved from malate by malic enzyme. Accordingly, there is a low deuterium effect on both enzymes, thereby increasing their relative contribution to carbon fluxes as compared with the PDH. Fourth, the ^{13}C distribution after $^{13}CO_2$ labeling in D_2O showed (1) a lower enrichment in malate, consistent with the involvement of the PEPC that used less ^{13}C-enriched phospho*enol*pyruvate (due to the deuterium effect on photosynthetic assimilation), and (2) a depletion of the citrate pool, revealing the rate-limiting nature of citrate synthase for the entry of neosynthesized acetyl-CoA into the TCA cycle.

Such conclusions are consistent with published biochemical data already discussed in the introduction. In fact, pyruvate kinase has been found inhibited by dihydroxyacetone phosphate in the light (Lin et al., 1989). Furthermore, the PEPC is known to be activated by phosphorylation in the light (Duff and Chollet, 1995), and protein phosphorylation is not affected by deuterium (Stein et al., 1978; Zhou and Adams, 1997). In addition, 2-oxoglutarate dehydrogenase is believed (1) to compete with the PDH for acetyl-CoA molecules and the E3 subunit of the enzymatic complex (Dry and Wiskich, 1987; Budde et al., 1991; Millar et al., 1999) and (2) to be inhibited by the NADH redox poise (Igamberdiev and Gardeström, 2003) and pyruvate (Dry and Wiskich, 1985). In other words, the oxidation of 2-oxoglutarate by this enzyme is not favorable in the light, as its substrates are more efficiently consumed by competing enzymes.

There is currently no convincing evidence that citrate synthase is controlled by allosteric phosphorylated effectors or NAD(P)H (Wiegand and Remington, 1986) except for a weak inhibition by ATP at pH less than 8 (large K_i of 5 mmol L^{-1}; Iredale, 1979). Neither is citrate synthase activity (1) influenced by posttranslational modifications (Wiegand and Remington, 1986) or (2) limited by the amount of substrate acetyl-CoA. Acetyl-CoA synthesis by the PDH is believed to exceed consumption by the TCA (Tcherkez et al., 2005), and respiring mitochondria are thought to have very large acetyl-CoA/free CoA ratios (Budde et al., 1991). Nevertheless, it should be recognized that in vitro citrate synthase activities measured from leaf extracts have been found to be limited, with values as low as approximately 0.3 μmol m^{-2} s^{-1} in tobacco (*Nicotiana tabacum*), which is less than that of the PEPC (near 5 μmol m^{-2} s^{-1}) or the isocitrate dehydrogenase (1–2 μmol m^{-2} s^{-1}; Scheible et al., 2000). Quite importantly, citrate synthase is inhibited by citrate, with a K_i value of 3 to 5 mmol L^{-1} (Matsuoka and Srere, 1973). Plausibly, therefore, the involvement of citrate synthase as a limiting step (see above) stemmed from both the inhibition by and the contribution of night-stored [^{12}C]citrate (Fig. 4) that impeded neosynthesized citrate from entering the TCA cycle. Other studies have indeed suggested that citrate is mainly produced during the night and used in the subsequent light period (Scheible et al., 2000; for a specific discussion, see Tcherkez and Hodges, 2008).

The TCA Cycle Is Bidirectional

The low rates of pyruvate kinase, 2-oxoglutarate dehydrogenase, and citrate synthase activities in vivo were associated with the redirection of oxaloacetate molecules to malate and then fumarate (Fig. 4). As such, the TCA cycle appeared not to operate like a proper cycle but rather as two different and weakly connected branches fed by the PEPC and stored citrate. Such a scenario agrees with the distribution of the ^{13}C label after pyruvate or Glc labeling. In fact, fumarate could be labeled with [^{13}C]1-pyruvate but not [^{13}C]3-pyruvate, demonstrating that the entry of [^{13}C]acetyl-CoA into the TCA cycle was small and that the PEPC activity was responsible for fumarate accumulation (Fig. 5). Accordingly, such a pattern was weakly sensitive to D_2O due to the absence of a deuterium isotope effect on the PEPC. Conversely, succinate, 2-oxoglutarate, and citrate were labeled by [^{13}C]3-pyruvate while fumarate was not (Fig. 5). Unsurprisingly therefore, when plotted against each

other, fumarate and succinate had contrasting labeling patterns, with two main groups that coincided with ^{13}C labeling in succinate under [^{13}C]3-pyruvate feeding on the one hand and the disappearance of [^{13}C]succinate under other labeling conditions on the other hand (Fig. 6).

The TCA ''cycle'' thus appeared as noncyclic, due to the lack of metabolic connection between 2-oxoglutarate (or succinate) and fumarate. In such a framework, the role of the PEPC as an anapleurotic source for supplying oxaloacetate molecules to feed both fumarate accumulation and the small citrate synthase flux is critical. Other studies provided further evidence of this using either biochemical measurements or stable isotope abundances (for review, see Tcherkez and Hodges, 2008).

The cyclic nature of the TCA pathway is restored during the night. In fact, the night activity of the TCA cycle was associated with a larger D_2O effect on [^{13}C]3-pyruvate decarboxylation (Fig. 3). Accordingly, ^{14}C labeling and $^{14}CO_2$ evolution measurements also showed that, contrary to the light, leaf dark respiration is associated with the consumption of pyruvate by the TCA cycle (Gibbs and Beevers, 1955). That is, oxaloacetate is regenerated from citrate through the breakdown of pyruvate into CO_2. In addition, there was little effect of D_2O on the rate of night respiration (Fig. 2), indicating that enzymes with a low deuterium dependency were involved in CO_2 evolution after illumination, such as the malic enzyme. The latter has indeed been found to be involved in CO_2 production in *Ricinus communis* leaves after the light-to-dark transition; accordingly, the malate pool decreases and the PEPC activity is down-regulated in the dark (Gessler et al., 2009).

Rationale and Perspectives

The carbon flow restriction through the TCA cycle and the fragmentation of the latter into backward and forward segments reflect imperatives caused by the metabolic control upon illumination: (1) the inhibition of TCA enzymes such as isocitrate dehydrogenase by large redox ratios [NAD(P)H/NAD(P)] within the mitochondrial matrix (Gardeström and Wigge, 1988; Igamberdiev and Gardeström, 2003); (2) the decrease of the glycolytic input of acetyl-CoA molecules because of elevated ATP and triose phosphates and the inhibition of both the pyruvate kinase and the PDH; and (3) the apparent reduction of TCA cycle activity by high dihydroxyacetone phosphate-to-Glc phosphate ratios (Tcherkez et al., 2008). Quite similarly, it has been shown in baker's yeast (*Saccharomyces cerevisiae*) with ^{13}C fluxomics techniques under fermentation conditions (in which large NADH/NAD levels occur) that the TCA cycle is reorchestrated into two opposite branches, producing fumarate and 2-oxoglutarate (Camarasa et al., 2003). In leaves, the large NADH/NAD ratio is believed to be caused by photorespiratory Gly decarboxylation (Igamberdiev and Gardeström, 2003) and the export of excess reductive power from the chloroplast (Noctor et al., 2007).

As a consequence, organic acids such as malate and fumarate accumulate, and both the small influx of neosynthesized citrate and the citrate reserve are consumed. A major fate of such citrate molecules is certainly Glu, as evidenced by the quite large production of [^{13}C]Glu after [^{13}C]3-pyruvate feeding, as well as [^{13}C]GABA (through the GABA shunt; Figs. 4 and 5). That is, Glu is one major carbon sink to which TCA-related organic acids are channeled and, as such, nitrogen metabolism appears cornerstone for day respiratory carbon metabolism. Accordingly, malate and fumarate may act as counteranions for pH regulation during nitrate assimilation. This view is consistent with that of Scheible et al. (2000), who argued that diurnal changes in both transcript levels and TCA enzyme activities correlated with nitrogen (NH_3) availability. In addition, it has been shown in short-term manipulations of CO_2/O_2 ratios that the TCA cycle activity was higher when photorespiration increased, thereby responding to a larger need of Glu molecules for the NH_2 transfer cycle during the recovery of photorespiratory cycle intermediates (Tcherkez et al., 2008).

Our conclusions may have pervading consequences such that likely nitrogen assimilation (Glu production) weakly correlates to instantaneous carbon assimilation because of the buffering effect of stored citrate and the use of PEPC-derived oxaloacetate molecules for fumarate production. Further experimental assessment that uses simultaneous ^{15}N and ^{13}C labeling is thus needed and will be addressed in a subsequent study.

MATERIALS AND METHODS

Plant Material

Xanthium strumarium (Asteraceae) plants were grown in the greenhouse from seed in 100-mL pots of potting mix and transferred to 3-L pots after 2 weeks. Minimum photosynthetic photon flux density during a 16-h photoperiod was kept at approximately 400 μmol m^{-2} s^{-1} by supplementary lighting. Temperature and vapor pressure deficit were maintained at approximately 25.5°C/18.5°C and 1.4/1.2 kPa day/night, respectively. The carbon isotope composition ($\delta^{13}C$) of CO_2 in the greenhouse air was $-9.5‰ \pm 0.3‰$. The third or fourth leaves (from the apical bud) were used for all measurements.

Gas-Exchange Measurements

Open System (Photosynthesis and On-Line Carbon Isotope Discrimination)

The photosynthesis system is similar to that described by Tcherkez et al. (2008). Briefly, a purpose-built assimilation chamber was connected in parallel to the sample air hose of the LI-6400 (LI-COR). Leaf temperature was controlled at 21°C with a water bath and was measured with a copper-constantan thermocouple plugged to the thermocouple sensor connector of the LI-6400 chamber/infrared gas analyzer. Inlet air was adjusted to approximately 10 mmol mol^{-1} H_2O and passed through the chamber at a rate of 30 L h^{-1}, monitored by the LI-6400. Light (400 μmol m^{-2} s^{-1}) was supplied by light-emitting diodes (Spot-LED PE5730-904; Pearl Diffusion). Inlet CO_2 was obtained from a gas cylinder (Alphagaz N48; Air Liquide) with a $\delta^{13}C$ of $-45.3‰ \pm 0.2‰$. The outlet air of the chamber was regularly shunted and was sent to a sampling loop to measure the $^{13}C/^{12}C$ and $^{18}O/^{16}O$ isotope compo-

sition and thus the on-line isotopic discrimination (Δ_{obs}). The gas inside the loop was introduced into an NA-1500 elemental analyzer (EA; Carlo-Erba), as described by Tcherkez et al. (2005). When the isotopic analysis was triggered, the loop was shunted and the gas inside was introduced into the EA with helium for gas chromatography. The connection valve between the EA and the isotope ratio mass spectrometer (Optima; GV Instruments) was opened when the CO_2 peak emerged from the EA. Δ_{obs} during photosynthesis was measured following the method described by Evans et al. (1986). The isotope composition of dark-respired CO_2 was similarly measured with the open system.

Sampling

Leaves were cut (petiole under water) at the end of the light period in the greenhouse and incubated in the dark (15 h) in either H_2O or D_2O at 21°C. Such an incubation period of 15 h allowed the full replacement of leaf water by D_2O and was enough for accumulated dark respiratory intermediates (such as citrate) to be fully deuterated (the proton/deuteron exchange time is about $0.4–0.7 \times 10^{-3}$ s at ambient temperature). The light was then turned on. Two types of ^{13}C-labeling experiments were carried out: 99% ^{13}C enrichments followed by NMR analyses, and near-natural ^{13}C abundance enrichments coupled to isotope-ratio mass spectrometry. The photosynthetic conditions were exactly similar in both (light level, temperature, O_2 and CO_2 mole fraction). In all experiments, photosynthesis was allowed to stabilize for 100 min before labeling, and then leaves were labeled for 2 h ([^{13}C]Glc and [^{13}C]pyruvate labeling) or 50 min ($^{13}CO_2$ labeling). For NMR analyses, the leaf was immediately frozen at the end of the labeling period with a freeze-clamp system and then kept at −80°C. Such a modest duration of $^{13}CO_2$ labeling (50 min) avoided the general buildup of ^{13}C signals and so allowed the accurate identification and quantification of ^{13}C peaks by NMR. Separate identical experiments were carried out for isotopic isotope-ratio mass spectrometry measurements, because in the latter case, the ^{13}C enrichment in labeling substrates (Glc and pyruvate) was lower (near-natural abundance) and the carbon isotope composition of dark-respired CO_2 was measured after illumination on dark-adapted leaves (30 min after the light was switched off).

*Day Respiration Rate and Γ**

The day respiration rate and Γ* were measured with the Laisk method (Laisk, 1977). Γ* values obtained in D_2O were corrected for the solvent isotope effect associated with CO_2 and O_2 dissolution in water ($\alpha_{H/D}$ of 0.994 and 1.097, respectively; Wilhelm et al., 1977; Scharlin and Battino, 1992).

NMR Analyses

NMR measurements were carried out as described by Tcherkez et al. (2005) from perchloric acid extracts prepared from 2.5 g of frozen leaf material. Spectra were obtained using a Bruker spectrometer (AMX 400) equipped with a 10-mm multinuclear probe tuned at 100.6 MHz (^{13}C-NMR). The assignment of ^{13}C resonance peaks was carried out according to Gout et al. (1993). Identified compounds were quantified from the area of their resonance peaks using fully relaxed conditions for spectra acquisition (pulses at 20-s intervals). Peak intensities were normalized to a known amount of the internal reference compound (maleate for ^{13}C) that was added to the sample (internal standard). When ^{13}C-^{13}C or ^{13}C-D spin-spin interactions occurred, the total ^{13}C signal of the C-atom position of interest was the sum of the peak intensities of the multiplet. Two types of control were done for NMR analyses: experiments with water (no labeling substrates) and those with ^{12}C substrate. The latter control was required to normalize the ^{13}C signal after ^{13}C labeling so as to calculate the ^{13}C percentage.

Chemicals

Heavy water (D_2O 99.9%; D-175 CDN-isotopes) was from Cluzeau Info Labo. D_2O was also enriched in ^{18}O at a near-natural abundance level ($\delta^{18}O = +668‰ \pm 5‰$ versus SMOW). The positional ^{13}C-labeled molecules (99% ^{13}C in the considered position) were purchased from Eurisotop. Pyruvate was dissolved in distilled water, and the pH was adjusted to 6.7 with NaOH. To obtain nonfully labeled solutions (near-natural abundances for Δ_{obs} experiments), the labeled compounds were mixed with industrial pyruvate ($\delta^{13}C = -21‰$) from Sigma. The resulting overall composition of pyruvate solutions was checked to be 1,400‰. In all case, the final concentration was 0.015 mol L^{-1}. The solutions were fed to leaves through the transpiration stream.

Calculations

The procedure used to calculate the decarboxylation rates of ^{13}C-enriched substrates in the light from apparent Δ_{obs} values has already been explained in detail by Tcherkez et al. (2005, 2008). Briefly, the difference between apparent Δ_{obs} values obtained with and without substrate addition is considered to reflect the additional decarboxylation flux in the light. Using mass balance equations, it can be shown that the decarboxylation rate r_{day} has the following form:

$$r_{day} = \frac{d}{SV_M} \cdot \frac{c_o\lambda_o - c_e\lambda_e + (c_e - c_o)\lambda_{fixed}}{\lambda_s - \lambda_{fixed}}$$

where d is airflow, S is leaf surface area, V_M is the molar volume at air temperature, and c_e and c_o are the CO_2 mole fractions in inlet and outlet air, respectively. λ values are ^{13}C percentages (using δ values is not possible because of large ^{13}C enrichments) in inlet CO_2 (subscript e), outlet CO_2 (subscript o), net fixed CO_2 (subscript fixed), and ^{13}C-enriched added substrate (subscript s). This equation holds for homogeneously labeled substrates; it is somewhat changed for positional enrichments to take into account the different origin of decarboxylated CO_2. This occurs when pyruvate is added: the C-1 atom of pyruvate is decarboxylated by PDH, while the C-2 and C-3 positions are decarboxylated by the TCA cycle.

A similar procedure applies to dark-respired CO_2 measurements. In other words, CO_2 that is produced in darkness (^{13}C percentage; λ_{global}) after a light period with ^{13}C-enriched substrate feeding comes from respiratory oxidation of new photosynthates (the ^{13}C percentage in the net fixed carbon; λ_{fixed}), photosynthates from the previous light period in the greenhouse (^{13}C percentage; $\lambda_{previous}$), and additional C coming from the ^{13}C-enriched substrate fed to the leaf (^{13}C percentage; λ_s). The night decarboxylation rate has the following form:

$$r_{night} = R_n \cdot \frac{\lambda_{global} - \lambda_P}{\lambda_s - \lambda_P}$$

where λ_p is a linear combination of $\lambda_{previous}$ and λ_{fixed}. R_n is the dark respiration rate. It is equal to $0.6\,\lambda_{previous} + 0.4\,\lambda_{fixed}$ after 2 to 3 h in the light under ordinary CO_2/O_2 conditions (during which 200–400 mmol C m^{-2} have been fixed; Nogués et al., 2004). It should be noted that possible variations in these coefficients only introduce negligible errors in the estimate of the ^{13}C-enriched substrate decarboxylation (r_{night}) because of the strong ^{13}C enrichment of the substrate (i.e. the λ_p value is always very small compared to λ_{global} or λ_s and may be neglected). Again, that relationship is somewhat modified with positional enrichments to take into account the different origin of decarboxylated CO_2 (Tcherkez et al., 2005).

Oxygen Isotope Calculations

The oxygen isotope fractionation ($^{18}\Delta_{obs}$) was measured on-line as described above. The oxygen isotope composition ($\delta^{18}O$, versus SMOW) of natural (H_2O) and heavy (D_2O) water used here was $-24‰ \pm 0.4‰$ and $+668‰ \pm 5‰$. The $\delta^{18}O$ value of water at the evaporative sites (δ_e) was back-estimated from $^{18}\Delta_{obs}$ with the following equations (Flanagan et al., 1991):

$$\delta_e = \frac{\Delta_{ea}(1 - \delta_a) + \delta_a - \varepsilon_w}{1 + \varepsilon_w}$$

where ε_w is the $^{16}O/^{18}O$ isotope fractionation factor associated with H_2O-CO_2 oxygen exchange (41.9‰ at 21°C). δ_a is the $\delta^{18}O$ value of water vapor in air. Δ_{ea} is the ^{18}O enrichment of leaf water compared with water vapor in air. If we assume a full ^{18}O isotopic equilibrium between H_2O and CO_2, we have:

$$^{18}\Delta_{obs} = \frac{a - \gamma\Delta_{ea}}{1 - \gamma\Delta_{ea}}$$

that rearranges to:

$$\Delta_{ea} = \frac{^{18}\Delta_{obs} - a}{\gamma(^{18}\Delta_{obs} - 1)}$$

where γ is the ratio $c_c/(c_a - c_c)$, with c_a and c_c being the CO_2 mole fraction outside the leaf and in mesophyll cells. a is the $^{16}O/^{18}O$ isotope fractionation

associated with CO_2 diffusion. As inlet air was completely dry in the gas exchange system used here, the water vapor in outlet air only came from transpired water. We thus made the further assumption (mass balance): $\delta_a \approx \delta_e - \varepsilon^+$, where ε^+ is the $^{16}O/^{18}O$ isotope fractionation factor associated with the liquid-vapor water equilibrium (−9.5‰ at 21°C). This gives:

$$\delta_e = \frac{\Delta_{ea}(1+\varepsilon^+) - \varepsilon^+ - \varepsilon_w}{\Delta_{ea} + \varepsilon_w}$$

The value of Δ_{ea} was obtained from $^{18}\Delta_{obs}$ (equation above) and the c_c value estimated with the internal mesophyll conductance measured in both natural and heavy water by Tcherkez and Farquhar (2008).

Metabolomic Measurements

Gas chromatography coupled to time-of-flight mass spectrometry was performed on a LECO Pegasus III with an Agilent 6890 N gas chromatography system and an Agilent 7683 automatic liquid sampler. The column was an RTX-5 w/integra-Guard (30 m × 0.25 mm i.d. + 10-m integrated guard column; Restek). Leaf samples (20 mg of powder from freeze-dried material) were ground in a mortar in liquid N_2 and then in 2 mL of 80% methanol in which ribitol (100 μmol L^{-1}) was added as an internal standard. Extracts were transferred to 2-mL Eppendorf tubes and centrifuged at 10,000*g* and 4°C for 15 min. Supernatants were transferred to fresh tubes and centrifuged again. Several aliquots of each extract (0.1 mL, 3 × 0.2 mL, and 0.4 mL) were spin-dried under vacuum and stored at −80°C until analysis. Methoxyamine was dissolved in pyridine at 20 mg mL^{-1}, and 50 μL of this mixture was used to dissolve the dry sample (from the 0.2-mL aliquot; see above). Following vigorous mixing, samples were incubated for 90 min at 30°C with shaking. Eighty microliters of *N*-methyl-*N*-(trimethyl-silyl)trifluoroacetamide was then added, and the mixture was vortexed and incubated for 30 min at 37°C with shaking. The derivatization mix was then incubated for 2 h at room temperature. Before loading into the gas chromatography autosampler, a mix of a series of eight alkanes (chain lengths of C_{10}–C_{36}) was included.

Analyses were performed by injecting 1 μL in splitless mode at 230°C injector temperature. The chromatographic separation was performed in helium as a carrier gas at 1 mL min^{-1} in the constant flow mode and using a temperature ramp ranging from 80°C to 330°C between 2 and 18 min, followed by 6 min at 330°C. The total run time per injection was 30 min. Ionization was made by electron impact at 70 eV, and the mass spectra acquisition rate was 20 spectra s^{-1} over the m/z range 80 to 500, as described previously (Weckwerth et al., 2004). Peak identity was established by comparison of the fragmentation pattern with mass spectra available databases (National Institute of Standards and Technology), using a match cutoff criterion of 700/1,000, and by retention index using the alkane series as retention standards. The integration of peaks was performed using the LECO Pegasus software. Because automated peak integration was occasionally erroneous, integration was verified manually for each compound in all analyses.

Clustering Analysis

The ^{13}C-NMR data were represented as an isotopomic array as described by Tcherkez et al. (2007). The positional isotopic abundances (in ^{13}C percentage) relative to the natural ^{13}C abundance (1.1%) are indicated by colors, so that black cells indicate near-natural abundance and green and red cells indicate lower and larger than natural ^{13}C abundance. The clustering analysis was carried out with MeV 4.1 software (Saeed et al., 2003) and based on the cosine correlation method.

Fluxomics Calculations from NMR Data

In the following, we describe how flux rates (here expressed as probability coefficients) associated with the reactions of respiratory metabolism have been calculated from ^{13}C signals (measured with NMR) in C-atom positions of metabolites. In other words, the ^{13}C signals were used as input variables and a set of equations (as described below) was used to calculate probability coefficients. The principle of the computation was to minimize residuals (sum of squares).

As this study used ^{13}C pulse experiments and not steady-state isotopic labeling, fluxomics calculations were based on ^{13}C amounts brought out by ^{13}C labeling (denoted as u_i for any C-atom position i) and not ^{13}C percentages. That is, the ^{13}C signal obtained with the control $^{12}CO_2$ experiment (denoted as $^{12}u_i$) was subtracted from that obtained with the $^{13}CO_2$ experiment (denoted as $^{13}u_i$): $u_i = {}^{13}u_i - {}^{12}u_i$. $^{12}u_i$ is ordinarily not equal to zero simply because of the natural ^{13}C abundance (1.1%). The ^{13}C amount brought by labeling was then normalized with the total assimilated ^{13}C (denoted as U). The corresponding value is denoted as P_i:

$$P_i = \frac{{}^{13}u_i - {}^{12}u_i}{U}$$

where i is the C-atom position of interest. Similarly, U is the total ^{13}C amount brought by the labeling; that is, $U = {}^{13}U - {}^{12}U$. The ^{13}C distribution (set of p_i values for all detected C-atom positions in NMR spectra) was then analyzed using a set of equations similar to those of Dieuaide-Noubhani et al. (1995) and Rontein et al. (2002) and exemplified by the equation below. We did not use flux rates here but instead probability coefficients from source C to the C-atom position i: any metabolic reaction j was associated with a probability coefficient (transfer coefficient) F_j. The transfer probability through two subsequent reactions, j and k, is assumed to be equal to the product F_jF_k. The probability that the ^{13}C signal of a C-atom position within a given metabolite was detected not only depends on the production rate but is also the result of its commitment into the subsequent reaction m; as such, we used $(1 - F_m)$ as a multiplying factor. For example, the C-1 atom position in pyruvate (Pyr) is formed through either glycolysis from triose phosphates (TP) or the malic enzyme from malate (Mal). We thus obtained the calculated ^{13}C amount brought by labeling (p_i) as follows:

$$p_1(\mathrm{Pyr}) = [p_1(\mathrm{TP})F_{gly}F_{pk} + p_1(\mathrm{Mal})F_{me}] \times (1 - F_{pdh})$$

where F_{gly}, F_{pk}, F_{me}, and F_{pdh} are the transfer coefficients associated with glycolytic PEP production, pyruvate kinase, malic enzyme, and pyruvate dehydrogenase, respectively. Similar equations were written for the other metabolites, so that the general equation for the C-atom position i of metabolite x is:

$$p_i(x) = f_i^x(F_j, p_k, y)$$

where F_j, p_k, and y are transfer coefficients, ^{13}C amounts, and other C-atom positions, respectively. f_i^x is the particular mathematical function associated with the position i in x. The F_j values were computed with the method derived from Römisch-Margl et al. (2007); that is, by minimizing the sum of squares:

$$S = \sum_i (P_i(x) - p_i(x))^2$$

where $P_i(x)$ is the observed value of the ^{13}C amount in C-atom position i in metabolite x.

Supplemental Data

The following materials are available in the online version of this article.

Supplemental Table S1. H/D isotope effects of the enzymes of interest.

Received June 17, 2009; accepted August 10, 2009; published August 12, 2009.

LITERATURE CITED

Atkin OK, Millar AH, Gärdestrom P, Day DA (2000) Photosynthesis, carbohydrate metabolism and respiration in leaves of higher plants. *In* RC Leegood, TD Sharkey, S von Caemmerer, eds, Photosynthesis, Physiology and Metabolism. Kluwer Academic Publishers, London, pp 203–220

Breker L, Weber H, Griengl H, Ribbons DW (1999) *In situ* proton-NMR analyses of *E. coli* HB101 fermentations in ^1H_2O and D_2O. Microbiology **145:** 3389–3397

Budde RJA, Fang TK, Randall DD, Miernyk JA (1991) Acetyl-coenzyme A can regulate activity of the mitochondrial pyruvate dehydrogenase complex in situ. Plant Physiol **95:** 131–136

Budde RJA, Randall DD (1990) Pea leaf mitochondrial PDH complex is inactivated *in vivo* in a light-dependent manner. Proc Natl Acad Sci USA **87:** 673–676

Bykova NV, Keerberg O, Pärnik T, Bauwe H, Gardeström P (2005) Interaction between photorespiration and respiration in transgenic potato plants with antisense reduction in glycine decarboxylase. Planta **222:** 130–140

Camarasa C, Grivet JP, Dequin S (2003) Investigation by ^{13}C-NMR and tricarboxylic acid (TCA) deletion mutant analysis of pathways for succinate formation in Saccharomyces cerevisiae during anaerobic fermentation. Microbiology **149:** 2669–2678

Day DD, Neuburger M, Douce R (1985) Biochemical characterization of chlorophyll-free mitochondria from pea leaves. Aust J Plant Physiol **12:** 119–130

Dieuaide-Noubhani M, Raffard G, Canioni P, Pradet A, Raymond P (1995) Quantification of compartmented metabolic fluxes in maize root tips using isotope distribution from C-13 or C-14 labeled glucose. J Biol Chem **270:** 13147–13159

Dry IB, Wiskich JT (1985) Inhibition of 2-oxoglutarate oxidation in plant mitochondria by pyruvate. Biochem Biophys Res Commun **133:** 397–403

Dry IB, Wiskich JT (1987) 2-Oxoglutarate dehydrogenase and pyruvate dehydrogenase activities in plant mitochondria: interaction via a common coenzyme A pool. Arch Biochem Biophys **257:** 92–99

Duff SMG, Chollet R (1995) In vivo regulation of wheat-leaf phospho-*enol*pyruvate carboxylase by reversible phosphorylation. Plant Physiol **107:** 775–782

Evans JR, Sharkey TD, Berry JA, Farquhar GD (1986) Carbon isotope discrimination measured concurrently with gas exchange to investigate CO_2 diffusion in leaves of higher plants. Aust J Plant Physiol **13:** 281–292

Flanagan LB, Bain JF, Ehleringer JR (1991) Stable oxygen and hydrogen isotope composition of leaf water in C3 and C4 plant species under field conditions. Oecologia **88:** 394–400

Gardeström P, Wigge B (1988) Influence of photorespiration on ATP/ADP ratios in the chloroplasts, mitochondria, and cytosol, studied by rapid fractionation of barley (*Hordeum vulgare*) protoplasts. Plant Physiol **88:** 69–76

Gessler A, Tcherkez G, Karyanto O, Keitel C, Ferrio JP, Ghashghaie J, Farquhar GD (2009) On the metabolic origin of the carbon isotope composition of CO_2 evolved from darkened light-acclimated leaves in Ricinus communis. New Phytol **181:** 385–398

Gibbs M, Beevers H (1955) Glucose dissimilation in the higher plant: effect of age of tissue. Plant Physiol **30:** 343–347

Gout E, Bligny R, Pascal N, Douce R (1993) The C-13 nuclear magnetic resonance studies of malate and citrate synthesis and compartmentation in higher plant cells. J Biol Chem **286:** 3986–3992

Hanning I, Heldt HW (1993) On the function of mitochondrial metabolism during photosynthesis in spinach (*Spinacia oleracea* L.) leaves. Plant Physiol **103:** 1147–1154

Hochuli M, Szyperski T, Wüthrich K (2000) Deuterium isotope effect on the central carbon metabolism of *E. coli* cells grown on a D_2O-containing medium. J Biomol NMR **17:** 33–42

Igamberdiev AU, Gardeström P (2003) Regulation of NAD and NADP dependent isocitrate dehydrogenases by reduction levels of pyridine nucleosides in mitochondria and cytosol of pea leaves. Biochim Biophys Acta **1606:** 117–125

Iredale SE (1979) Properties of citrate synthase from *Pisum sativum* mitochondria. Phytochemistry **18:** 1057–1059

Kasimova MR, Grigiene J, Krab K, Hagedorn PH, Flyvbjerg H, Andersen PE, Möller IM (2006) The free NADH concentration is kept constant in plant mitochondria under different metabolic conditions. Plant Cell **18:** 688–698

Krömer S (1995) Respiration during photosynthesis. Annu Rev Plant Physiol Plant Mol Biol **46:** 45–70

Laisk AK (1977) Kinetics of Photosynthesis and Photorespiration in C_3 Plants. Nauka, Moscow

Lawlor DW (2002) Carbon and nitrogen assimilation in relation to yield: mechanisms are the key to understanding production systems. J Exp Bot **53:** 773–787

Lin M, Turpin DH, Plaxton WC (1989) Pyruvate kinase isozymes from the green alga *Selenastrum minutum*: kinetic and regulatory properties. Arch Biochem Biophys **269:** 228–238

Matsuoka Y, Srere PA (1973) Kinetic studies of citrate synthase from rat kidney and rat brain. J Biol Chem **248:** 8022–8030

Millar AH, Hill SA, Leaver CJ (1999) Plant mitochondrial 2-oxoglutarate dehydrogenase complex: purification and characterisation in potato. Biochem J **343:** 327–334

Noctor G, De Paepe R, Foyer CH (2007) Mitochondrial redox biology and homeostasis in plants. Trends Plant Sci **12:** 125–134

Nogués S, Tcherkez G, Cornic G, Ghashghaie J (2004) Respiratory carbon metabolism following illumination in intact French bean leaves using $^{13}C/^{12}C$ isotope labeling. Plant Physiol **136:** 3245–3254

Nunes-Nesi A, Sweetlove LJ, Fernie AR (2007) Operation and function of the tricarboxylic acid cycle in the illuminated leaf. Physiol Plant **129:** 45–56

Rasmusson AG, Escobar MA (2007) Light and diurnal regulation of plant respiratory gene expression. Physiol Plant **129:** 57–67

Römisch-Margl W, Schramek N, Radykewitz T, Hettenhuber C, Eylert E, Huber C, Römisch-Margl L, Schwarz C, Dobner M, Demmel N, et al (2007) $^{13}CO_2$ as a universal metabolic tracer in isotopologue perturbation experiments. Phytochemistry **68:** 2273–2289

Rontein D, Dieuaide-Noubhani M, Dufourc EJ, Raymond P, Rolin D (2002) The metabolic architecture of plant cells: stability of central metabolism and flexibility of anabolic pathways during the growth cycle of tomato cells. J Biol Chem **277:** 43948–43960

Rose IA (1961) The use of kinetic isotope effects in the study of metabolic control. J Biol Chem **236:** 603–609

Rose IA, Kellermeyer R, Stjernholm R, Wood HG (1962) The distribution of ^{14}C in glycogen from deuterated glycerol-^{14}C as a measure of the effectiveness of triosephosphate isomerase *in vivo*. J Biol Chem **237:** 3325–3331

Saeed AI, Sharov V, White J, Li J, Liang W, Bhagabati N, Braisted J, Klapa M, Currier T, Thiagarajan M, et al (2003) TM4: a free, open-source system for microarray data management and analysis. Biotechniques **34:** 374–378

Scharlin P, Battino R (1992) Solubility of 13 non-polar gases in deuterium oxide at 15-45°C and 101.325 kPa: thermodynamics of transfer of non-polar gases from H_2O to D_2O. J Solution Chem **21:** 67–91

Scheible WR, Krapp A, Stitt M (2000) Reciprocal diurnal changes of PEPc expression, cytosolic pyruvate kinase, citrate synthase and NADP-isocitrate dehydrogenase expression regulate organic acid metabolism during nitrate assimilation in tobacco leaves. Plant Cell Environ **23:** 1155–1167

Stein RL, Romero R, Bull HG, Cordes EH (1978) A kinetic α-deuterium isotope effect for the binding of purine nucleosides to calf spleen purine nucleoside phosphorylase: evidence for catalysis by distortion. J Am Chem Soc **100:** 6249–6251

Tcherkez G, Cornic G, Bligny R, Gout E, Ghashghaie J (2005) In vivo respiratory metabolism of illuminated leaves. Plant Physiol **138:** 1596–1606

Tcherkez G, Cornic G, Bligny R, Gout E, Mahé A, Hodges M (2008) Respiratory metabolism of illuminated leaves depends on CO_2 and O_2 conditions. Proc Natl Acad Sci USA **105:** 797–802

Tcherkez G, Farquhar GD (2008) On the effect of heavy water (D_2O) on carbon isotope fractionation in photosynthesis. Funct Plant Biol **35:** 201–212

Tcherkez G, Ghashghaie J, Griffiths H (2007) Methods for improving the visualization and deconvolution of isotopic signals. Plant Cell Environ **30:** 887–891

Tcherkez G, Hodges M (2008) How isotopes may help to elucidate primary nitrogen metabolism and its interactions with (photo)respiration in C3 leaves. J Exp Bot **59:** 1685–1693

Tovar-Mendez A, Miernyk JA, Randall DD (2003) Regulation of pyruvate dehydrogenase complex activity in plant cells. Eur J Biochem **270:** 1043–1049

Weckwerth W, Wenzel K, Fiehn O (2004) Process for the integrated extraction, identification and quantification of metabolites, proteins and RNA to reveal their co-regulation in biochemical networks. Proteomics **4:** 78–83

Wiegand G, Remington SJ (1986) Citrate synthase: structure, control and mechanism. Annu Rev Biophys Biophys Chem **15:** 97–117

Wilhelm E, Battino R, Wilcock RJ (1977) Low-pressure solubility of gases in liquid water. Chem Rev **77:** 219–262

Zhou J, Adams JA (1997) Is there a catalytic base in the active site of cAMP dependent protein kinase? Biochemistry **36:** 2977–2984